Research Article Vol. 62, No. 15 / 20 May 2023 / Applied Optics 4017

applied optics

Humidity-insensitive optical fibers for distributed sensing applications

Tiago F. P. Neves,[1,2,*] Lorenzo Scherino,[1] Rémy Bernard,[3] Monika Bouet,[3] Aymeric Pastre,[3] Regina Magalhães,[4] Sonia Martin-Lopez,[4] Hugo F. Martins,[5] Paolo Petagna,[1] and Luc Thévenaz[2]

[1]Experimental Department, Detector Technology Group, CERN - European Organization for Nuclear Research, CH-1211 Geneva, Switzerland
[2]EPFL - Swiss Federal Institute of Technology, Group for Fibre Optics, SCI-STI-LT Station 11, 1015 Lausanne, Switzerland
[3]Univ-Lille, CNRS, UMR 8523 - PhLAM - Physique des Lasers Atomes et Molécules, F-59000 Lille, France
[4]Departamento de Electrónica, Universidad de Alcalá, 28805, Alcalá de Henares (Madrid), Spain
[5]Instituto de Óptica, Consejo Superior de Investigaciones Científicas, 28006 Madrid, Spain
*tiago.neves@fibersight.pt

Received 15 February 2023; revised 7 April 2023; accepted 21 April 2023; posted 24 April 2023; published 17 May 2023

Humidity is a critical environmental factor in various applications, and its temperature dependence must be considered when developing thermo-hygrometer fiber sensors. The optical fibers that constitute the sensor must have a temperature reference, which should be resistant to humidity to avoid cross-sensitivities. This paper presents two innovative optical fibers insensitive to humidity over temperatures ranging from −20°C to 55°C. To the best of our knowledge, the novel standard size optical fibers coated with acrylate and silicone are tested under controlled conditions using an optical time-domain reflectometer sensor based on Rayleigh scattering. The sensor achieves meter-range resolution over kilometers of length with a response time of few minutes.

https://doi.org/10.1364/AO.487264

1. INTRODUCTION

Distributed optical fiber sensors (DOFS) are employed in a wide variety of applications such as temperature, strain, pressure, or vibration monitoring. Their popularity has increased significantly mainly due to the possibility of having accurate real-time local information over a wide detection range using a single interrogation unit and optical fiber [1]. These systems provide a cost-effective alternative to complex point optical fiber sensors (OFS) arrays because the monitoring detection range can be extended to hundreds of kilometers with a spatial resolution that can vary from a few millimeters to a few meters [2,3].

Most of optical fibers are composed of a core surrounded by a cladding and externally protected by a coating. Light is trapped inside the core and guided along its entire length due to the difference in refractive index between core and cladding. The outer surface of an uncoated optical fiber, when exposed to air, moisture, or other hazards, may exhibit flaws over the glass surface. Initially, such defects may be microscopic but, over time, they may turn into larger cracks that impact the mechanical resistance of the optical fiber. Therefore, coatings play a key role in protecting the fiber from the atmospheric environment, but they also absorb any light that is not properly guided.

A standard telecommunications fiber (ITU-T G.652) is usually coated by two layers of acrylate polymer. The inner coating layer, with a diameter around 180 μm, is a soft polymer that mitigates the effects of micro-bending on the fiber, while the outer layer, with 250 μm of diameter, is a hard-shell polymer that protects the fiber from the external environment. More recently, depending on the application environment where the fiber is installed, different materials such as polyimide, carbon or composite structures are used as fiber coatings [4]. In harsher environments, the fiber is protected with additional layers of coating made of materials as aluminum or strong plastics.

Although one of the functions of the coating is to protect the optical fiber from humidity [5], most of them are generally composed of a polymeric material and react significantly to humidity variations. The coating swells when absorbing humidity and shrinks when desorbing it, inducing strain into the fiber body and thus core [6]. The effects of humidity on commercial polyimide- and acrylate-coated optical fibers was previously studied by several authors [7–9] and, while the polyimide coating shows a higher and more stable sensitivity to humidity, the response of the acrylate to humidity is not negligible and should be investigated to avoid cross-sensitivities between temperature and humidity. Due to the cross-sensitivities, the main challenge ahead and objective of this work is to decouple the temperature and humidity effects in a distributed fiber sensor.

Different decoupling techniques can be carried out, such as using two parallel sensing fibers with different temperature and relative humidity (RH) sensitivities [10,11], or using a

completely stripped fiber for temperature reference [12]. One last technique is to completely isolate the fiber using a metallic sheath, to block the humidity absorption by the fibers coating, and turn it into a pure temperature reference. The first solution is valid and takes advantage from the fact that both fibers experience the same environmental conditions. With this technique, the measurement resolution always depends on the ratio between the two fibers sensitivities, and if the difference is not significant, the system may turn ill-conditioned showing large uncertainties. The second decoupling solution using a stripped fiber, solves the uncertainty problem, because the reference fiber is completely insensitive to RH, but raises another limiting issue that is the fragility of the fiber. Using a completely stripped fiber only works in extremely controlled environments, which is unrealistic for in-field applications. The third one, using a fiber sheath against humidity, reduces the ease of handling and increases significantly the cost of the fiber, mostly because it increases the manufacturing complexity.

The focus of this work is to identify a coated fiber that is insensitive to RH at different temperatures, as this would be the optimal solution for decoupling temperature and humidity effects. This is a crucial issue to tackle to improve the accuracy and reliability of DOFS in a wide range of humidity applications. Such an optical fiber should be coated to be resistant for in-field applications and would be used as a temperature reference in a thermo-hygrometric distributed fiber sensor. In this work, two innovative solutions for solving the cross-sensitivity issue are presented. The first one is based on a novel optical fiber with a single layer of a specific acrylate coating, the Desolite DS3471-3-14, that combines the properties of soft and hard coating, meaning that the fiber is significantly mitigating microbending and, simultaneously, it is mechanically protected. The choice of this polymer coating is due to its low dynamic water sensitivity (DWS), enabling increased fiber drawing speeds and offering improved humidity resistance [13]. Several Desolite-coated fibers with different coating thicknesses were produced to fully investigate the RH effect at temperatures from −20°C to 50°C, using a chirped-pulse phase-sensitive optical time domain reflectometer (CP-ϕ-OTDR) interrogator [14]. The second solution presents a new kind of silicone-coated optical fiber that was chosen based on the high capacity of water repellency and good releasability of the silicone material [15]. Seven samples, 1 m each, were produced and tested at different temperatures from −20°C to 55°C using a frequency-scanned ϕ-OTDR interrogator [12]. It is here demonstrated that two of the Desolite-coated optical fibers tested secure a total RH insensitivity above 15°C and maintain a very reduced RH sensitivity below this temperature level, while the silicone-coated optical fibers present a complete immunity to humidity variations in the temperature range from −20°C to 55°C.

A. Fundamentals of Distributed Optical Fiber Sensors

The fundamental mechanism of distributed optical fiber sensors is based on the light scattering effects, which are affected by changes applied to the optical fiber, typically temperature and strain. Such physical changes will turn encoded onto the scattered light, which conveys them up to the detection stage where it is processed to be spatially resolved. In a dense homogeneous medium, as a perfect crystal at zero absolute temperature, the molecules are arranged in a very regular way and the medium's response is the same in every position. Due to the symmetric structure, all the scattering waves mutually cancel out for all angles except in the forward propagation. In this case, there is no scattering but just a change in the overall velocity of propagation [16]. However, if the medium is non-homogeneous, such as glass, the medium's response varies randomly, causing different orthogonal scattering components that do not mutually cancel completely. Each molecule acts as a scattering center and any imperfection in the structure modifies the optical properties and results in lateral and backscattering waves.

The great majority of existing DOFS are based on three scattering mechanisms: Rayleigh and Brillouin scattering, where the backscattered signal inside the material is directly dependent on temperature and stress applied on the fiber; and Raman, where the backscattered signal only depends on the temperature [17]. Temperature variations influence the thermal expansion and thermo-optic coefficients of the fiber materials, while the applied stress influences the photo-elastic coefficient. The three scattering mechanisms can have two flavors: spontaneous and stimulated. When the input light does not significantly affect the properties of the medium, the scattering is linear and labeled as spontaneous. In contrast, if the light intensity increases to a level where the optical properties of the medium are modified and the scattered light efficiency is proportional to the power of the input light, the scattering is considered stimulated and enters into a non-linear regime [18]. Because the Raman effect is only sensitive to temperature and the Brillouin effect presents a significantly lower sensitivity, when compared to the Rayleigh effect, this work is based on Rayleigh backscattering, which occurs when the optical power is transferred from the incident to the scattered wave keeping the same original frequency [19,20].

A Rayleigh-based DOFS can be realized by techniques such as optical time-domain reflectometry (OTDR) [21] or optical frequency-domain reflectometry (OFDR) [22]. The detection principle is based on launching a light pulse in an optical fiber cable and collecting the backscattered light at the same fiber end. The pulse round trip results in a trace and each point of the trace corresponds to one section of the fiber. In a traditional OTDR, which is mostly used for measuring the fiber signal attenuation and monitor the fiber links in communication networks, the Rayleigh backscattered signal is analyzed in the time domain and provides a meter or sub-meter spatial resolution over tens of kilometers. In an OFDR system, which can have a sub-millimeter spatial resolution but limited to some meters of sensing range, the light source frequency is linearly changed, by changing the input current laser. This means that the spatial resolution of an OFDR depends on the frequency tuning range of the interrogation light rather than the detector bandwidth, as it happens in an OTDR. A standard OTDR uses a low coherence optical source and measures the intensity of the reflected light. It requires a high-power broadband incoherent source and a long acquisition time due to the weak Rayleigh signal. This method is most generally used by the telecommunications industry to locate anomalous points in the optical fiber cable. However, if the light source used in the setup is a highly coherent optical pulse, the system is called ϕ-OTDR.

B. ϕ-OTDR Technique

The ϕ-OTDR technique interrogates an optical fiber through the propagation of a sequence of rectangular optical pulses [23]. In this case, the laser coherence length is longer than the distance between two consecutive reflector centers and the total backscattered signal does not only depend on the intensity reflected by each center, but also on the phase interference of the total backscattered field present in each fiber section. The backscattered light from the different scattering points interferes within the pulse width and results in a randomly varying signal in time, which is highly dependent on the optical frequency and the refractive index. This signal can be exactly reproduced under the same experimental conditions of temperature, strain, and optical frequency [24]. The ϕ-OTDR interrogation technique measures the noise-like but static Rayleigh backscattered signal caused by the frozen and random longitudinal entropic fluctuations of the refractive index (RI) alongside the optical fiber [25]. The optical fiber should be seen as a series of closely packed RI discontinuities and each one causes a tiny and random amount of reflection. This method takes a photograph of the optical fiber's core structure to have the fiber pattern that changes randomly if a perturbation occurs.

This paper focuses on two variants of ϕ-OTDR technique, the first being called frequency-scanned and the second chirped pulse. A frequency-scanned ϕ-OTDR technique requires acquiring repeatedly the Rayleigh scattering intensity traces by sweeping the carrier optical frequency of the optical pulse. Each fiber position will be individually analyzed at different frequencies and, if the fiber is subjected to any change of temperature or strain, which changes its RI, the local spectrum will equivalently experience a frequency shift. The spectrum frequency shift is generally estimated using techniques of cross-correlation between the two spectral distributions. It results in a correlation peak located at a frequency shift proportional to the local temperature or strain variations.

A deterministic spectral shift of these random signal variations can be also caused by the stress induced by the deformed coating in presence of water molecules. The humidity causes an expansion/contraction of the coating, stressing the fiber, and if the fiber is free of static mechanical strain, the total backscattered signal is only a function of the temperature and humidity. With a temperature reference, the humidity can be easily measured and the total strain variation $\Delta\varepsilon_{\text{total}}$ is given by the following equation:

$$\Delta\varepsilon_{\text{total}} = (1 - P_e)\Delta RH + [(1 - P_e)\alpha + \xi]\Delta T, \quad \textbf{(1)}$$

where P_e is the photo-elastic coefficient of the optical fiber, α and ξ are the thermal expansion and thermal optic coefficients respectively, ΔT the temperature and ΔRH the relative humidity.

On the other side, if the probe pulse has a linear frequency variation along the pulse width, the system is called CP-ϕ-OTDR, which is, nowadays, a fast, powerful, and highly sensitive refractive index sensor for distributed acoustic sensing (DAS) [14]. The CP-ϕ-OTDR interrogator technique relies on the same working principle of ϕ-OTDR but instead of sweeping the laser frequencies, it produces a linear chirp with different frequencies that generates the same trace pattern for the same fiber. The method achieves spatial resolutions in the meter range, with an increasing signal-to-noise (SNR) by several orders of magnitude with respect to the conventional ϕ-OTDR technique [26]. Typically, a picosecond probe optical pulse is amplified and time stretched before launching it into the fiber under test (FUT). CP-ϕ-OTDR avoids the need of rigorous acoustic and thermal stabilization, because the measurements are based on a single-shot pulse rather than a large laser frequency sweeping. Simultaneously, it does not need a laser source with a large linewidth and eliminates the fading problems generated when the scattering of a single position is extremely low. The Rayleigh scattering is formed by the superposition of the waves generated by the random photons in each section and if the input light pulses have always the same power, as it happens in a traditional ϕ-OTDR, statistically the scattering random pattern has significant fluctuations in the power that may have some values near zero fading the signal [27]. However, when using probe pulses whose power is varying over its width, the modulation instability-induced by the signal fading is significantly reduced [28]. In contrast, the spatial resolution is limited to the meter range because of the weak Rayleigh intensity traces, and the bandwidth required at the receiver is the same as the coherent detection, limiting the maximum measurements range.

2. EXPERIMENTAL RESULTS

The results section is divided into two parts, each addressing the results for a specific type of coating (Desolite-coated and silicone-coated optical fibers).

A. Desolite-coated Optical Fiber

1. *Fibers Under Test*

All Desolite-coated fibers used in this study were entirely manufactured at FiberTech Lille (IRCICA-Université de Lille) by drawing & modified chemical vapor deposition (MCVD) silica glass preform doped with germanium and phosphorus oxide, on which the coating was immediately applied during drawing. The resulting SMF-type fiber showed a core-to-cladding diameter ratio of 8/125 with a refractive index difference of about 6×10^{-3} between core and cladding. The attenuation coefficient was 0.5 dB/km at 1550 nm, as measured using an OTDR. A 4-μm-core-diameter fiber protected by a Desolite coating was also manufactured. To obtain a well-known RH reference during the test, a polyimide-coated optical fiber was also inserted among the tested fibers. The temperature reference is given by a stripped coated fiber (bare) and all of these fibers have been spliced and serially arranged to form a single FUT, held strain free in special plastic holder, as shown in Fig. 1. The FUT was around 770 m long and made of six pieces of Desolite-coated fibers (The fibers designations are provided by the manufacturer.) with different thicknesses (from 26.5 to 93.5 μm); one piece of Desolite-coated fiber with a thin identical coating (27.5 μm) but with a 4 μm core diameter; one piece of polyimide-coated commercial fibers; and one piece of bare silica fiber. The full list of FUT with specs is detailed in Table 1.

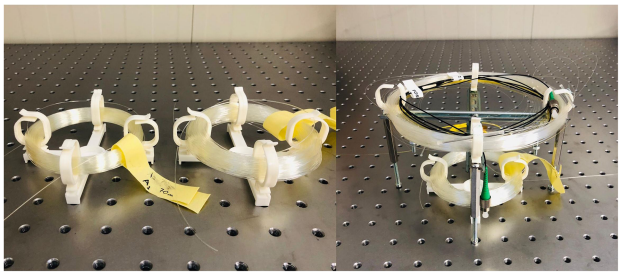

Fig. 1. Desolite-coated fiber in stress-free holders.

Table 1. List of FUT with Their Respective Coating and Core Characteristics

Fiber	Coating Type	Coating Thickness (μm)	Core Diameter (μm)
A	DS3471-3-14	27.5	4
E1	DS3471-3-14	26.5	8
C1	DS3471-3-14	55.5	8
A1	DS3471-3-14	57.5	8
B1	DS3471-3-14	63.5	8
F1	DS3471-3-14	85.0	8
G1	DS3471-3-14	93.5	8
PI	Polyimide	15	9
B	Bare	0	9

2. Climatic Chamber

The set of tests was performed in a climatic chamber developed at European Organization for Nuclear Research (CERN) and specially prepared to work at a very low RH with a resolution of 0.1% of RH. The temperature ranges from −20°C to 55°C. A photo of the climatic chamber setup can be seen in Fig. 2. Figure 3 shows the full schematic of the climatic chamber.

The temperature control is performed using a refrigerated-heating circulator (Julabo FP-50), while the RH control is ensured by a pneumatic circuit that mixes dry and wet air flows. Different combinations of both flows create different levels of humidity, and they are controlled by two electronic mass flow controllers (MFC) (Bronkhorst El-Flow). The connection with the outside is performed through high-vacuum feedthrough connectors for both optical fibers and copper wires, which enables a stable control over the humidity level in the chamber below a dew point of −60°C. The climatic chamber enables to precisely control the RH from 0% up to 90% and can be monitored and controlled remotely. As a reference RH sensor, a chilled mirror dew point hygrometer (EdgeTech DewMaster)

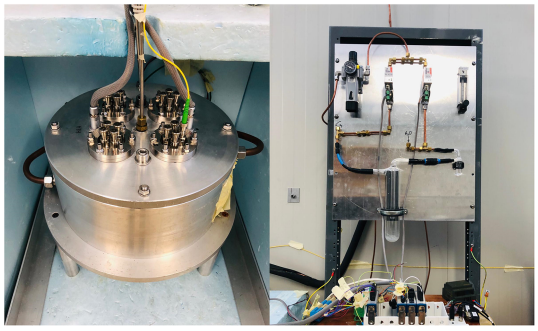

Fig. 2. Photos of CERN climatic chamber and pneumatic circuit.

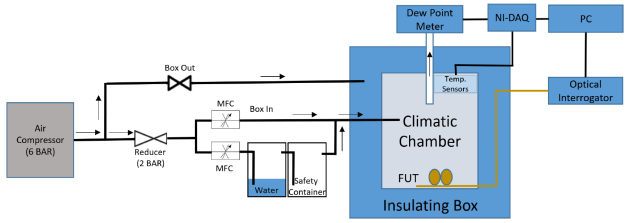

Fig. 3. Schematic of the climatic chamber including the pneumatic circuit and the electronic data acquisition system. MFC, mass flow controller.

was used, while three calibrated resistance thermometers (PT100) were used as temperature reference. LabVIEW software makes the interface between the National Instruments data acquisition module (NI-DAQ), where all the reference sensors are connected, and the PC. The design of the climatic chamber also provides protection to the fibers against mechanical disturbances caused by vibration.

3. Optical Interrogator

The initial set of measurements was conducted with a CP-ϕ-OTDR interrogator, which was the only available option in the lab at that time. However, later in the study, the unavailability of the CP-ϕ-OTDR interrogator and the requirement for improved spatial resolution led to the adoption of a frequency-scanned ϕ-OTDR. The FUT is connected to a CP-ϕ-OTDR interrogator, represented in Fig. 4 and its detailed description can be found in [29–31]. The instrument was provided by Dpto. de Electrónica, Universidad de Alcalá, Madrid, Spain.

An external cavity laser (ECL) emits monochromatic CW light with an optical frequency that can be linearly swept by driving the laser using an electrical current ramp. This frequency-swept light is then shaped into an optical pulse by a semiconductor optical amplifier (SOA). The SOA is synchronized with the ECL driver, and the output signal power is amplified by an erbium-doped fiber amplifier (EDFA). The resulting probe is injected into the FUT through an optical circulator and the backscattering signal is amplified before the photodetector (PD). Two variable optical attenuators (VOA) are placed before the FUT and before the PD, the first to prevent non-linear effects caused by an intense optical pulse and the second to avoid the PD power saturation limit. Two band pass filters (BPF) are used to reduce the amount of transmitted EDFA spontaneous emission. For this test, the spatial resolution

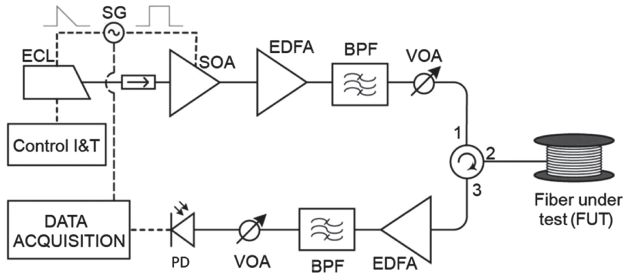

Fig. 4. Schematic of a CP-ϕ-OTDR interrogator. ECL, external cavity laser. SG, signal generator. SOA, semiconductor optical amplifier. EDFA, erbium-doped fiber amplifier. BPF, band pass filters. VOA, variable optical attenuator. PD, photo detector [26].

was set to 6 m, giving a frequency accuracy on the maximum correlation determination below 1 MHz, which corresponds to approximately 1 mK of temperature shift. To address the typical performance challenges of CP-ϕ-OTDR systems, including the risk of substantial errors and reduced long-term referencing accuracy, optimization techniques have been implemented, such as restricting the frequency range to a maximum of 4% of the chirp bandwidth and taking the average of 40 acquired traces. To further minimize cumulative long-term errors, the optical reference trace is updated whenever a local disturbance is equivalent to a 4% shift of the total chirp bandwidth.

4. Temperature Characterization

The experimental procedure started with a temperature characterization followed by six RH tests at different constant temperatures (−20°C, −10°C, 0°C, 15°C, 25°C and 50°C).

The temperature was gradually changed from 25°C to −20°C at a constant level of RH (7.3% ± 0.5%) to avoid cross-sensitivities. Figure 5 shows temperature and RH measured by the reference sensors in A), the fibers frequency shift in B), the respective temperature calibrations in C), and the variation of the temperature sensitivity with the coating thickness in D).

The first observation is that all fibers show linear temperature dependence, with a coefficient of determination (R^2) always higher than 0.99. The polyimide-coated and the bare fiber results confirm what was obtained in [9], with a temperature sensitivity of 1.31 GHz/K and 1.12 GHz/K, respectively. All temperature sensitivities are summarized in Table 2.

Table 2. FUT with Thicknesses and Temperature Sensitivities

Fiber	Coating Thickness (μm)	S_T (GHz/K)	R^2
A	27.5	1.279 ± 0.008	0.9999
E1	26.5	1.193 ± 0.008	0.9999
C1	55.5	1.30 ± 0.03	0.9979
A1	57.5	1.31 ± 0.04	0.9978
B1	63.5	1.34 ± 0.04	0.9968
F1	85.0	1.43 ± 0.06	0.9939
G1	93.5	1.48 ± 0.08	0.9922
PI	15	1.31 ± 0.01	0.9998
B	0	1.12 ± 0.01	0.9998

The bare fiber shows the lowest temperature sensitivity, due to the absence of extra thermal stress owing to coating and the temperature sensitivity of the Desolite-coated fibers, increases linearly with the coating thickness, as seen in Fig. 5(D).

The uncertainty of the temperature sensitivity also increases with the coating thickness, as expressed by the lower R^2. Fibers that have a thinner coating tend to exhibit better linear fitting as the stress generated by the coating is minimal when compared to the stress caused by the thermal expansion of the silica glass. As the thickness of the coating increases, the stress induced by it also increases. Overall, the uncertainty on the temperature sensitivity is of the order of tens of MHz/K.

The smaller core diameter of fiber A resulted in less accurate splicing with the previous fiber, causing significant signal loss and temperature sensitivity issues (not considered in Fig. 5(D)). To prevent further signal loss to the remaining fibers, fiber A was

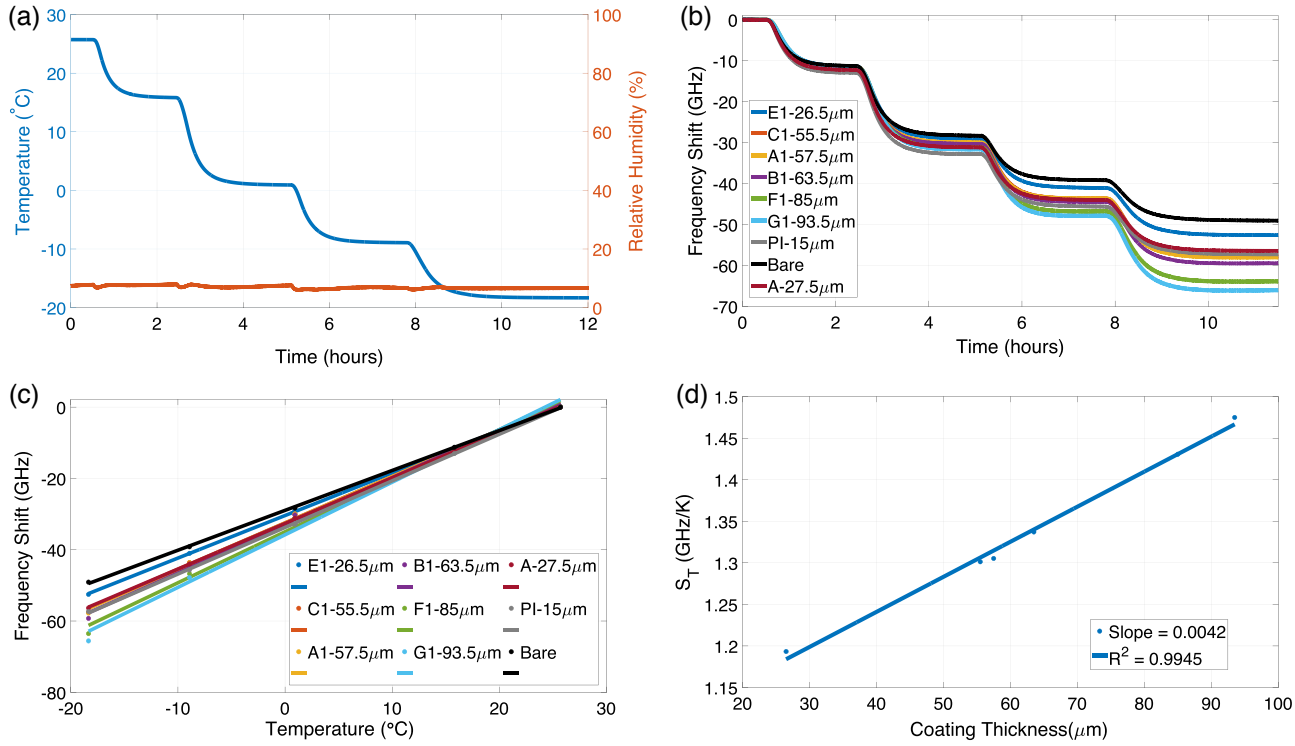

Fig. 5. (a) Climatic chamber conditions during the temperature characterization test. Temperature in blue and RH in orange. (b) Grouped plot of all fibers frequency shift during the temperature characterization test. (c) Temperature calibrations plot of all fibers. (d) Variation of the temperature sensitivity, S_T, with the coating diameter.

placed at the end of the chain. However fiber A shows a linear temperature response (1.279 GHz/K). Up to 93.5 μm of coating diameter, the temperature sensitivity of the Desolite-coated fibers increases linearly at a rate of 4.2 MHz/K/μm.

5. Relative Humidity Characterization

The RH calibration is performed after applying a temperature compensation method to remove the residual temperature variation inside the climatic chamber. The total frequency shift (ΔF_{total}) measured for each fiber has a RH (ΔF_{RH}) and a temperature (ΔF_T) dependence. The temperature reference is given by the bare fiber (ΔF_{bare}), which is only sensitive to temperature, but as demonstrated in the previous section, the temperature sensitivity of the coated fibers is not the same as that of the bare fiber. For that reason, on top of the bare fiber frequency shift, a corrective factor should be applied to correct the temperature-compensation method. All fibers have linear temperature sensitivities, which means that a ratio between the two temperature sensitivities is sufficient to correct the measurement:

$$\Delta F_{\text{RH}} = \Delta F_{\text{total}} - \left(\frac{S_{T_{\text{fiber}}}}{S_{T_{\text{bare}}}} \times \Delta F_{\text{bare}} \right), \tag{2}$$

where $S_{T_{\text{fiber}}}$ and $S_{T_{\text{bare}}}$ are the temperature sensitivities of the selected fiber and bare fiber respectively. An example of this compensation method is given in Fig. 6 that shows the response of an acrylate-coated fiber during a RH test.

At the beginning of the test, there were oscillatory fluctuations measured by the acrylate-coated and bare fibers. That is clearly a temperature fluctuation in the climatic chamber, as seen in the temperature reference plot, and it is visible that after applying the compensation method, the compensated signal is completely immune to these temperature variations, proving that the compensation method is valid.

A RH test was performed afterwards at 50°C, 25°C, 15°C, 0°C, −10°C, and −20°C. Figure 7 groups the results at 25°C.

Figure 7(A) illustrates the temperature and RH dynamics during the test carried out at 25°C, monitored by the setup reference instrumentation, in which the RH was sequentially changed from 0.2% to around 80%. The responses of all fibers under test, already compensated to mitigate the temperature effect, are compared in Fig. 7(B). The first observation is that all

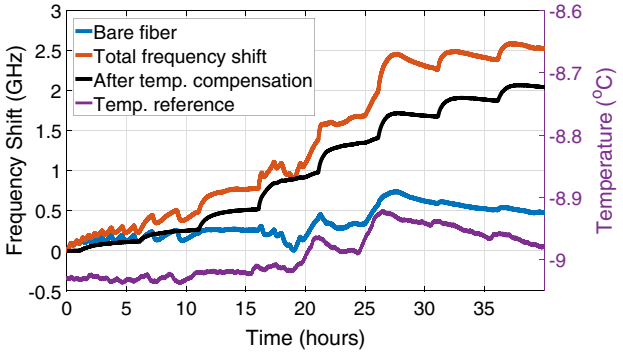

Fig. 6. Example of the temperature compensation method. The fiber total frequency shift is plotted in orange, the reference bare fiber in blue, and the compensated trace in black. The temperature reference is plotted in purple.

fibers have a completely negligible response to RH when compared with the polyimide-coated fiber. This RH insensitivity might be explained by the different DWS of polymer coatings [13]. The DWS parameter depends on the ability of porous material, such as polymers, to absorb water molecules, and it turns out to be smaller for the polymer Desolite DS 3471-3-14 than for other kinds of secondary coatings (Information provided by the manufacturer - on 150 μm films: weight change −2%; extractable −1%).

Analyzing only the Desolite-coated fibers, one can conclude that at 25°C, their responses are similar to the temperature reference, given by the bare fiber, and show a very minor dependence on RH variations. Figure 7(C) shows the comparison with the bare fiber, and it is clear that, even though the Desolite-coated fibers can be considered insensitive to RH and be used as a temperature reference at 25°C, their behavior differs slightly from the bare fiber. Except for fibers A and E1, whose responses are extremely close to the bare fiber, the responses of the thicker coated fibers at high RH values show a residual RH sensitivity that may be used for RH sensing, although at a much reduced magnitude. The temperature sensitivity is around 1.3 GHz/K, while the RH sensitivity is a few MHz/%RH. Figure 7(D) shows the RH calibrations of five fibers C1, A1, B1, F1, and G1. In this case, the RH sensitivity calibration curve is not linear. The best-fitting equation is a 2nd degree polynomial, and consequently, the RH sensitivity is a linear function of the RH itself. This non-linear behavior is explained by the non-linear variation of the Young's modulus, which scales the mechanical stiffness of a solid material. Young's Modulus, especially of the acrylate polymers, decreases linearly with increasing humidity and logarithmically with strain [32]. The combined effects of these parameters, humidity and strain rate, results in a non-linear RH response. Simultaneously, the temperature has a significant impact on the Young's Modulus of this kind of DS3471 coating. It varies from 2.2 MPa at 20°C to 520 MPa at −60°C [33]. Consequently, it is expected that a fiber with this kind of coating changes drastically its behavior at different temperatures. In contrast, this effect is not evident in the PI-coated fibers because the variation of Young's modulus in the tested temperature range is not significant (3.2 ± 0.1 GPa) [34].

A RH test at 50°C was performed afterwards. Figure 8(A) shows the climatic chamber dynamics during the test and due to limitations in the testing setup, it was not possible to go beyond 20% RH at 50°C. Figure 8(B) groups the frequency shift of all the tested fibers. Comparing the Desolite-coated fibers with the PI fiber response, after applying the temperature compensation method, it is clear that the Desolite-coated fiber responses are negligible, confirming that these fibers can also be used as temperature reference in an RH distributed sensor prototype operating at high temperatures. Figure 8(C) shows that the responses of the Desolite-coated fibers are similar to the bare fiber (black line) that, simultaneously, is similar to the temperature variations measured by the reference temperature sensors, as seen in Fig. 8(A). Until around 10 h of test, the climatic chamber was still significantly dry, and the RH variation was very small, around 2%. For that reason, none of the fibers absorbed water molecules and it explains the complete overlapping behavior with the bare fiber.

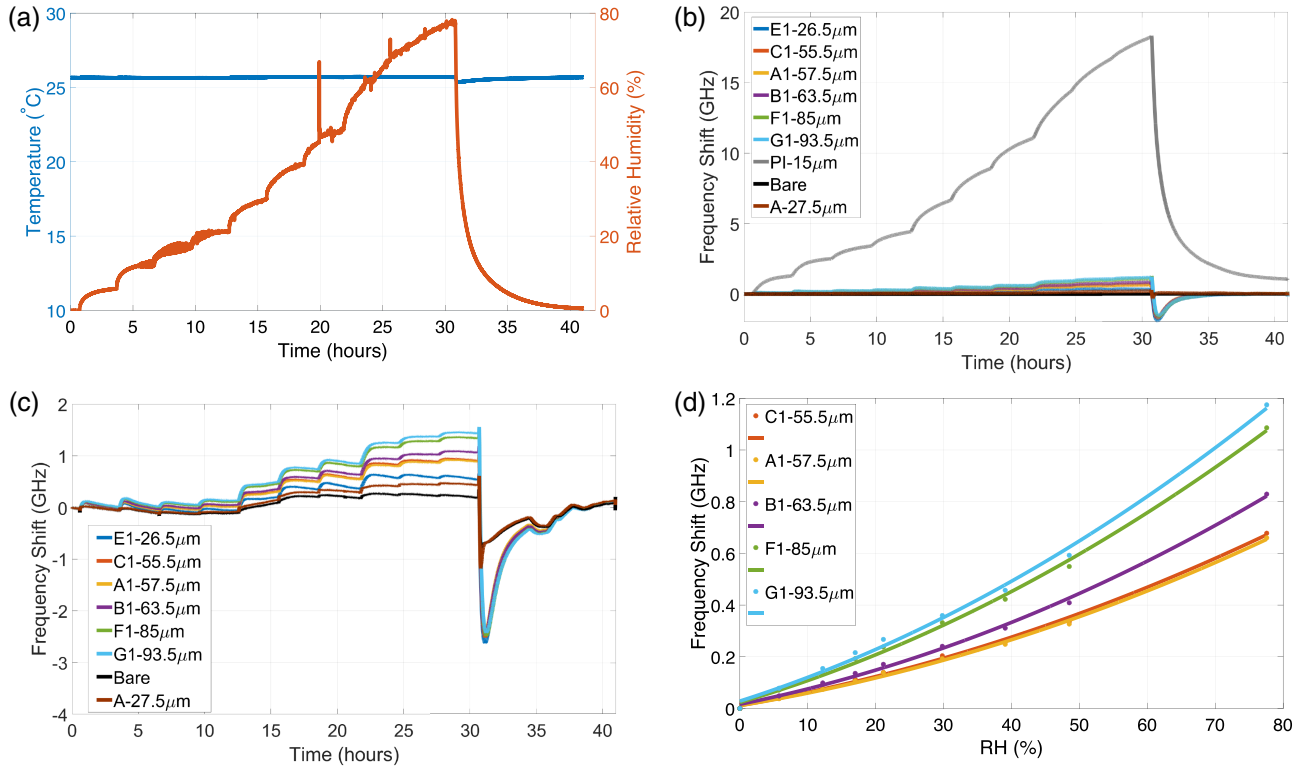

Fig. 7. (a) Climatic chamber conditions during the RH characterization test. Temperature in blue and RH in orange. (b) Grouped plot of the frequency shifts of all fibers during the RH characterization test. (c) Grouped plot of the frequency shift of all Desolite-coated fibers together with the bare fiber. (d) RH calibration of five Desolite-coated fibers.

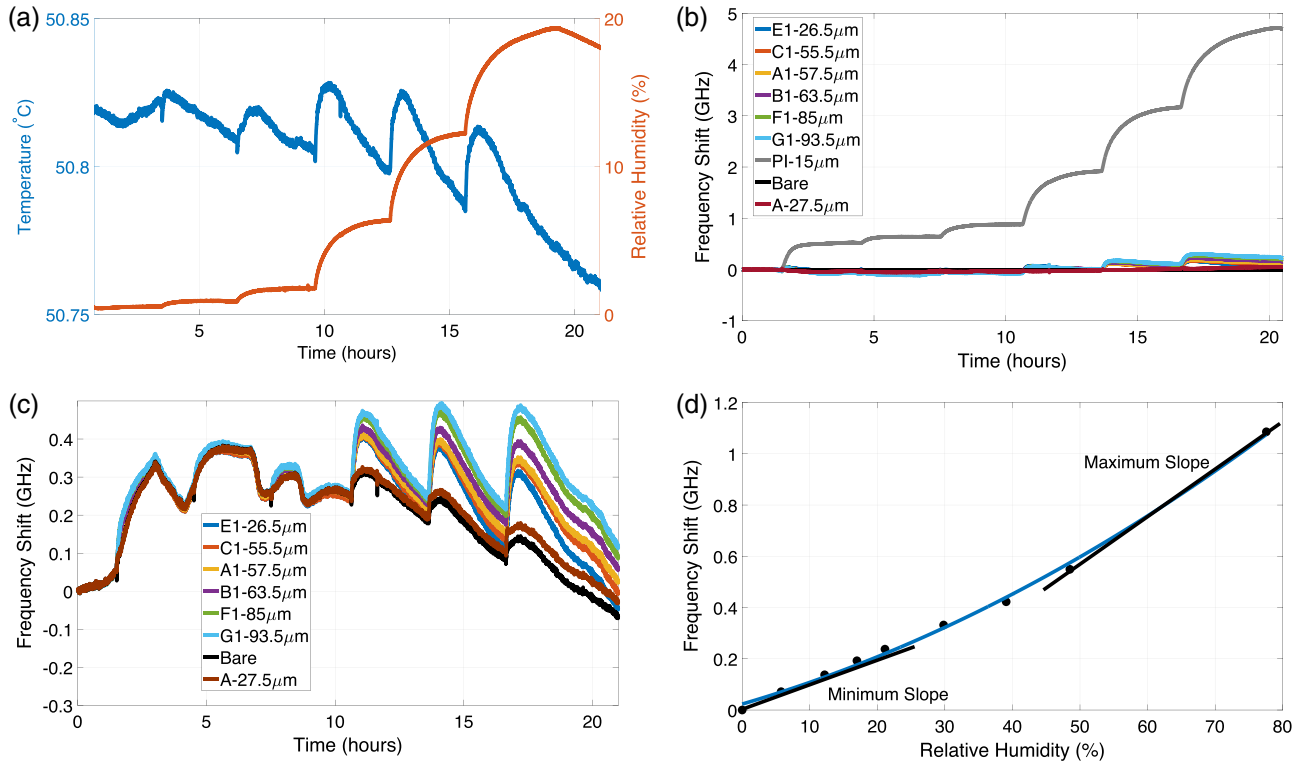

Fig. 8. (a) Climatic chamber conditions during the RH at 50°C. (b) Grouped plot of all fibers during the RH test at 50°C. (c) Grouped plot of Desolite-coated fibers frequency shift during the RH test at 50°C. (d) Example of minimum and maximum RH sensitivity.

Table 3. RH Sensitivities of All Fibers in MHZ/%RH[a]

Fiber	Thickness (μm)	50°C	25°C	15°C	0°C	−10°C	−20°C
A	27.5	INS.	INS.	2.9 ± 1.2	15.4 ± 8.6	32.7 ± 16.6	52.6 ± 7.8
E1	26.5	INS.	INS.	4.7 ± 0.6	18.0 ± 11.0	31.1 ± 14.7	44.5 ± 4.5
C1	55.5	INS.	9.3 ± 2.4	9.2 ± 2.1	36.2 ± 22.2	74.4 ± 36.0	96.4 ± 1.0
A1	57.5	INS.	9.0 ± 2.5	9.3 ± 1.9	35.2 ± 20.9	71.9 ± 33.2	100 ± 1.2
B1	63.5	INS.	11.5 ± 3.1	12.1 ± 2.7	42.3 ± 25.0	84.0 ± 37.3	110.8 ± 4.2
F1	85.0	INS.	15.5 ± 3.1	16.0 ± 4.4	53.3 ± 31.5	106.2 ± 39.6	137.1 ± 15.3
G1	93.5	INS.	16.65 ± 3.4	18.3 ± 5.4	61.7 ± 38.2	123.6 ± 49.5	156.2 ± 20.6
PI	15	220.9	236.2	229.5	227.6	223.4	184.3

[a]INS = Insensitive.

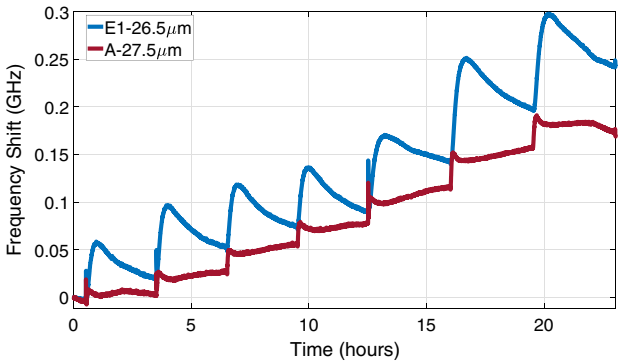

Fig. 9. Response of fiber A, in red, and E1, in blue, during a RH test at 15°C.

After 10 h, the humidity started to increase significantly. It is visible that in the latest RH steps, the thicker fibers show RH sensitivity. Nevertheless, the RH sensitivity is attenuated after a couple of hours and, it is predictable that waiting more time, the difference between the fibers responses and the bare fiber would be completely vanished. At 50°C, all Desolite-coated fibers show RH insensitivity.

As the Desolite-coated fibers show a non-linear RH response, the RH sensitivities comparison is not straightforward. In this study, to compare the RH sensitivities at different temperatures, a simplification was made. An example can be seen in Fig. 8(D). For every temperature tested, the minimum and the maximum RH sensitivity were calculated with the minimum and maximum linear slopes in the range of explored RH. The minimum and maximum slopes give the minimum and maximum RH sensitivity of each fiber at each temperature in the tested RH range. Then, the mean of both values is calculated, and the difference between the minimum or maximum values and the mean gives the measurement error.

At 15°C, the two less RH sensitive fibers, fiber A and E1, start to react slightly to RH, but with RH sensitivities of the same magnitude order as the optical interrogator error. When comparing the behaviors of these two fibers, it is possible to conclude that fiber E1 reacts to humidity changes, but it tends to return to a lower level, as shown in Fig. 9.

The magnitude of this effect is residual compared with the temperature sensitivity, but it can be seen as a small local spike in the temperature signal, which would then almost disappear. In contrast, fiber E1 tends to return to a lower level, and fiber A tends to slowly increase. A possible explanation for the different

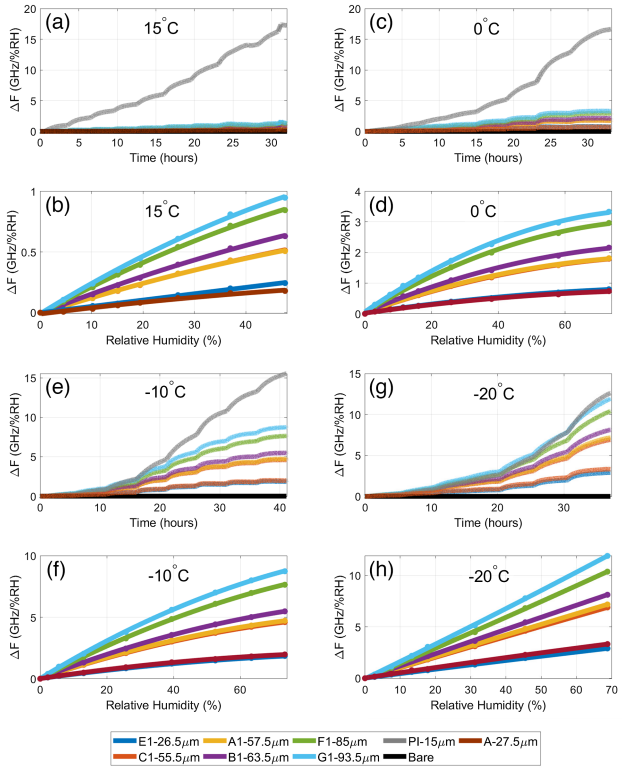

Fig. 10. Grouped plot of all fiber frequency shifts at different temperatures. (a) Frequency shift at 15°C. (b) RH calibrations a 15°C. (c) Frequency shift at 0°C. (d) RH calibrations a 0°C. (e) Frequency shift at −10°C. (f) RH calibrations a −10°C. (g) Frequency shift at −20°C. (h) RH calibrations at −20°C.

behavior of the two fibers could be that fiber A was manufactured with Desolite from a different batch and about 2 years earlier. The actual composition and even the curing process may have been changed slightly and its behavior may not be exactly the same as fiber E1. The results of all the remaining RH tests at different temperatures are grouped in Fig. 10, and Table 3 summarizes all RH sensitivities calculated in this study with the respective errors. The remaining Desolite-coated fibers show a higher RH sensitivity but still much smaller when compared with the polyimide-coated fiber. Decreasing the temperature, the RH response starts to increase significantly and at 0°C, the RH sensitivity of the thicker fibers is approximately half of the RH sensitivity of the polyimide-coated fiber. At −10°C, the RH sensitivities continue to increase, getting closer to the

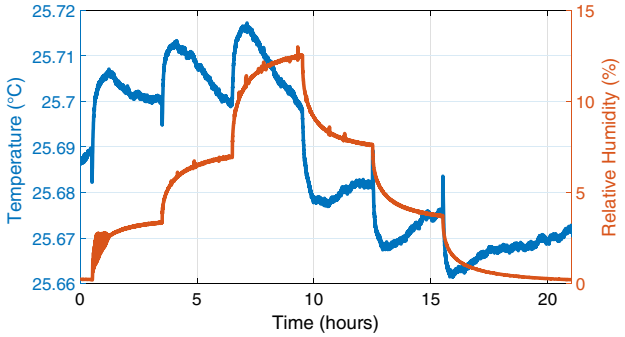

Fig. 11. Climatic chamber conditions in the four-step RH test at 25°C.

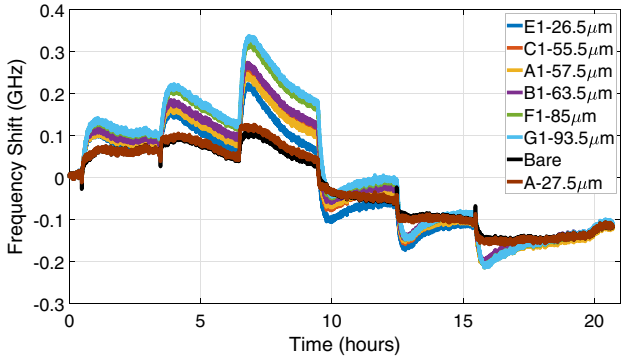

Fig. 12. Grouped plot of all Desolite-coated fibers during the four-step RH test at 25°C.

polyimide-coated fiber RH sensitivity. At −20°C, the thicker Desolite-coated fibers end up by showing a RH sensitivity to that in polyimide-coated fibers.

Although we cannot accurately estimate the response time of the optical fiber sensors, it is worth noting that their response time is not slower than that of the climatic chamber. However, given that the climatic chamber has a response time in the order of seconds, it is reasonable to infer that the optical fibers will also respond in a similar order of magnitude.

To explore further the RH effect on these fibers, a final four-step RH test at 25°C was performed. The test consisted of smaller RH changes, but with positive and negative variations to analyze the RH absorption and releasing behavior differences. The dynamics are represented in Fig. 11, and the frequency shift of all Desolite-coated fibers is presented in Fig. 12.

The main observation is that when the RH variation is of the order of 12%, the response of the Desolite-coated fibers matches the temperature change for either increasing or decreasing RH. As expected, the thicker fibers show some transient frequency shift, while fiber A, for example, is completely unaffected by the RH changes at 25°C.

6. Conclusion

The main conclusion of our work on Desolite-coated optical fibers so far is that they are good candidates to serve as temperature references in an RH distributed sensor, in particular fibers E1 and A. These two fibers can be considered RH insensitive at temperatures above 15°C. Below this temperature, the RH

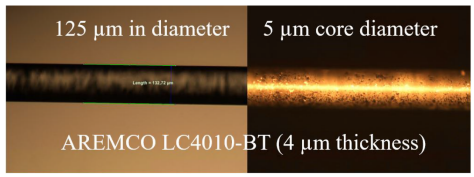

Fig. 13. Silicone-coated fibers micrograph.

sensitivity is still negligible. All the remaining fibers show an RH insensitivity at 50°C, but a significant RH sensitivity at temperatures below 0°C. At temperatures around 15°C, all fibers have an RH sensitivity between 1% and 10% of the PI fiber RH sensitivity, and for that reason, it can be considered negligible. At temperatures above 0°C, the fibers temperature sensitivity is a few orders of magnitude higher than the RH sensitivity and, for comparison reasons, even if the RH changes with 100% at 15°C, which is an extreme case, the equivalent change of temperature for fiber A is around 0.3°C. Even down to temperatures of −20°C, a significant variation of 20% of RH induces a temperature error around 0.7°C, which is a negligible error for most of the temperature applications. For the G1 fiber, at −20°C, a variation of 10% RH can induce an error of 1°C, which is already a significant variation. Coupling one of these Desolite-coated fibers, especially fiber A and E1, with a polyimide-coated fiber, a distributed thermo-hygrometer to operate at temperatures above 15°C can be developed with low cross-sensitivities issue.

B. Silicone-coated Optical Fibers

Regarding the restrictions mentioned in the previous section limiting the operation of a thermo-hygrometer at temperatures above 15°C, a RH insensitive fiber that would operate over a broader temperature range has to be ideally identified. One candidate is silicone owing to its well-known impermeability to water molecules [15], and several samples of silicone-coated fiber were drawn to address this issue.

1. Fibers under Test

The FUT is composed of seven identical silicone-coated fibers samples with a uniform thickness of 4 μm (The thickness was chosen to ensure the fiber's durability and RH insensitivity.) and a length of 1 m. A bare fiber and a polyimide-coated fiber were appended to the FUT to be the temperature and RH references during the test. The FUT was completed with a sample of a Desolite-coated fiber, fiber A−27.5 μm. All fibers were spliced and serially arranged to form a single compound fiber and subjected to tests of temperature and RH at four different temperatures, 25°C, 0°C, −15°C, and 55°C. To facilitate splicing and to clearly distinguish each fiber position, each sample was supplemented with a 1 m segment of standard fiber. Figures 13 and 14 show a micrograph and the fibers in a stress-free holder.

2. Climatic Chamber

The climatic chamber used in this study was already explained in Section 2.A.2.

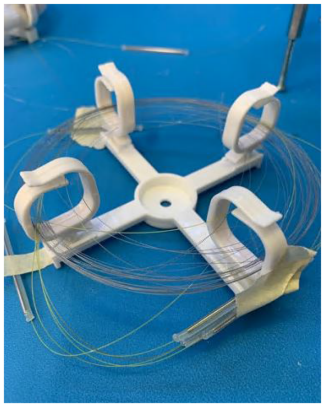

Fig. 14. Silicone-coated fibers in a stress-free holder.

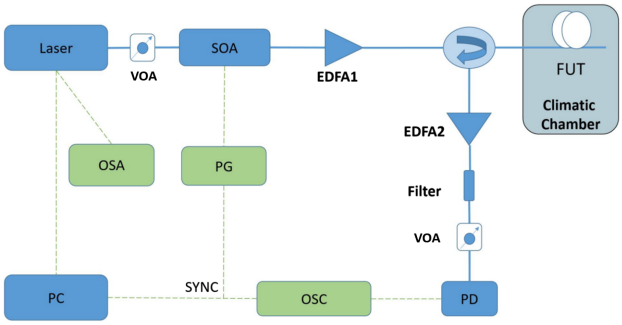

Fig. 15. Full schematic of the ϕ- OTDR setup. VOA, variable optical attenuator; SOA, semiconductor optical amplifier; EDFA, erbium-doped fiber amplifier; PD, photo detector; OSA, optical spectrum analyzer; PG, pulse generator; OSC, oscilloscope.

3. Optical Interrogator

In the second set of measurements, the use of the previous interrogator was not feasible as the silicone-coated fiber samples were 1 m each and its spatial resolution was limited to 6 m. Consequently, a new interrogator with improved accuracy and a spatial resolution of approximately 1 m was assembled and utilized. Given the 1 m spatial resolution of the interrogator and the fact that each sample is also 1 m in length, we only receive a single measurement per sample. The home-made optical interrogator used in this test is a frequency-scanned ϕ-OTDR, and its schematic is presented in Fig. 15.

A distributed feedback (DFB) laser with 1 MHz linewidth is employed as a laser source. Then, a SOA driven by a pulse generator is used to shape the continuous laser light into a coherent pulse. After the pulse shaping, an EDFA is used to amplify the pulse before launching it to the FUT through an optical circulator. The output of the circulator is connected to another EDFA, which amplifies the Rayleigh backscattered signal, and then, a tunable filter (1550 nm) is connected to filter out the EDFA amplified spontaneous emission before photodetection. The photodetector is then connected to a fast oscilloscope for data acquisition. An optical spectrum analyzer (OSA) is used to tune the filter to match the laser wavelength. A LabVIEW visual interface (VI) controls the laser current sweeping and acquires all the traces measured by the oscilloscope (OSC). Two variable optical attenuators are placed before the SOA and the PD, the first to prevent non-linear effects caused by a too intense optical pulse and the second to avoid the PD power saturation.

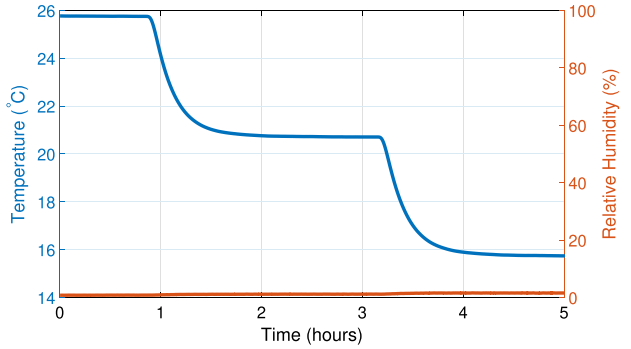

Fig. 16. Climatic chamber conditions during the three-step temperature characterization.

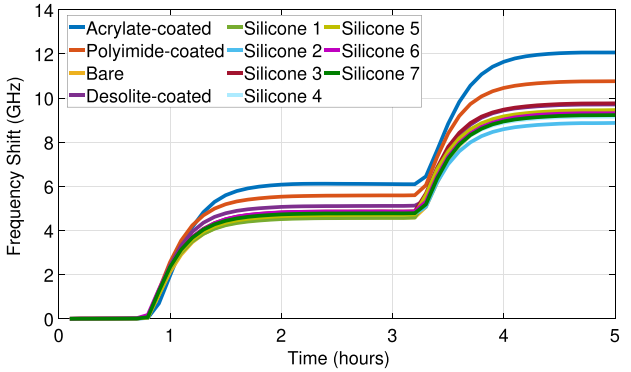

Fig. 17. Silicone-coated fibers compared with bare fiber in the temperature test.

4. Temperature Characterization

The objective of the three-step temperature characterization (25°C, 20°C, and 15°C) was to compare the behavior of these new silicone-coated fibers with the bare fiber. Figure 16 shows the climatic chamber dynamics during the test and Fig. 17 the response of the full FUT.

As illustrated in Fig. 17, the response of the silicone-coated fibers is nearly identical to that of the bare fiber and the Desolite-coated fibers, suggesting that the temperature sensitivity of these fibers is nearly the same with a maximum variation of ±5%. The response of the acrylate- and polyimide-coated fibers is higher, as demonstrated in the previous sections.

5. Relative Humidity Characterization

The RH characterization consisted in a RH test at five pre-set temperatures, 55°C, 25°C, 0°C, and −20°C. The results and were not temperature compensated to be able to compare them directly with the bare fiber results. Figure 18 groups the climatic chamber conditions, the response of all fibers, and a comparative plot with one silicone-coated fiber and bare fiber for the four tested temperatures. Despite the selection of different silicone-coated fibers for comparing with the bare fiber in

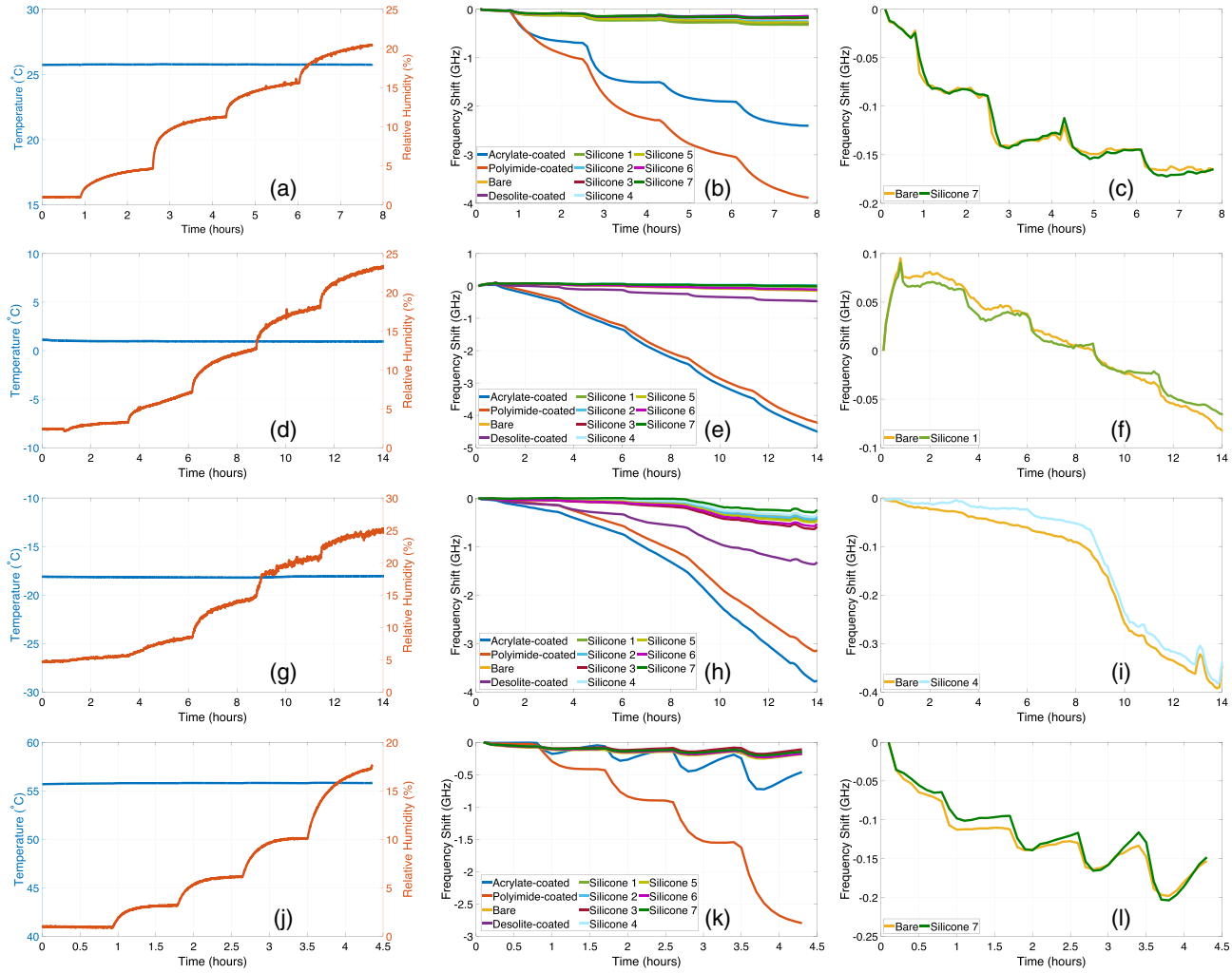

Fig. 18. (a) Climatic chamber conditions during the RH test at −20°C. (b) Silicone-coated fibers compared with bare fiber in the RH test at 25°C. (c) Silicone-coated fiber sample, in green, compared with bare fiber, in yellow, during the RH test at 25°C. (d) Climatic chamber conditions during the RH test at 0°C. (e) Frequency shifts of all fibers during the RH test at 0°C. (f) Silicone-coated fibers, in light green, compared with bare fiber, in yellow, during the RH test at 0°C. (g) Climatic chamber conditions during the RH test at −20°C. (h) Frequency shifts of all fibers during the RH test at −20°C. (i) Silicone-coated fibers, in light blue, compared with bare fiber, in yellow, during the RH test at −20°C. (j) Climatic chamber conditions during the RH at 55°C. (k) Silicone-coated fibers compared with bare fiber in the RH test at 55°C. (l) Silicone-coated fibers compared, in green, with bare fiber, in yellow, during the RH test at 55°C.

Figs. 18(C), 18(F), 18(I), and 18(L), the behavior of the remaining is remarkably similar, as evidenced by the data presented in Figs. 18(B), 18(E), 18(H), and 18(K).

The first RH test was performed at 25°C, and the results are shown in A, B, and C. The climatic chamber conditions are plotted in A, and as expected, the responses of the acrylate- and polyimide-coated fibers are higher due to their hygroscopic characteristics (B). (C) shows that the response of the silicone-coated fibers to RH is clearly negligible, and it is close to the bare fiber, which only measures the temperature fluctuation in the climatic chamber. A similar RH test was performed at 0°C, and the climatic conditions are shown in D, the frequency shifts of all fibers in E and the comparison of one silicone-coated sample with the bare fiber in F. At 0°C, the behaviors of the silicone-coated fibers and the bare fiber are again similar. At lower temperatures, the Desolite-coated fibers become RH sensitive, as seen in the previous sections, while the silicone-coated fibers remain completely insensitive. A similar analysis and similar results were obtained in an RH test at −20°C, presented in G, H, and I. At −20°C, the behavior of the silicone-coated fibers remains completely insensitive to RH, following the bare fiber. A final RH test at 55°C was also performed to complete the analysis of the silicone-coated fibers at higher temperatures. J, K, and L show the response of the full FUT during the RH test and the comparison between one silicone-coated sample and bare fiber, respectively. Again, the silicone-coated fibers appear immune to RH variations at 55°C.

6. Conclusion

This section proves that the silicone-coated fibers are, among all the coated optical fibers tested in this study, the best candidates to serve as a temperature reference in a thermo-hygrometer distributed fiber sensors. When coated with a thin layer of silicone,

Table 4. Comparison of Coating Thickness and Temperature Range for RH Insensitivity

Coating	Coating Thickness (μm)	RH Insensitivity
Desolite	26.5–27.5	15°C to 55°C
Silicone	4	−20°C to 55°C

the optical fiber shows the same response as a bare optical fiber, over the tested temperature range, while being protected with a coating. Silicone-coated fiber is a valid solution to solve the temperature-RH cross-sensitivities issue, as it can be considered as a fiber very immune to humidity influence.

3. CONCLUSIONS

The temperature-RH cross-sensitivities issue has an important impact on any thermo-hygrometer sensor, and the main conclusion of this study is that a valid solution for this issue has been found. Table 4 presents a summary of the coating characteristics and the corresponding temperature range where both of the selected optical fibers demonstrate complete insensitivity to variations in humidity.

In conclusion,

- Desolite-coated fibers are strong candidates for serving as temperature reference, in applications above 15°C. They are easy to manufacture and low cost. While some previous related works demonstrated that the standard acrylate-coated fibers present a non-negligible RH sensitivity from 30 to 200 MHz/%RH [9], fiber A or E1 present, for the same temperature range, a RH sensitivity ranges from 0 to 50 MHz/%RH.
- Silicone-coated fibers increase the range of temperatures over which the optical fibers are insensitive to RH. Between the temperature range of −20°C to 55°C, the sensor can be considered a pure temperature sensor with a high degree of reliability. This behavior is only comparable to that of coating-stripped optical fibers.

Funding. CERN, the European Organization for Nuclear Research; Ministère de l'Enseignement Supérieur et de la Recherche; Hauts-de-France Regional Council; European Regional Development Fund (CPER Photonics for Society, P4S); IRCICA, USR 3380, CNRS-Univ, F-59000 Lille, France; European Commission (FINESSE, MSCA-ITN-ETN-722509); Ministerio de Ciencia, Innovación y Universidades (IJCI-2017-33856, RTI2018-097957-B-C31, RTI2018-097957-B-C33); Comunidad de Madrid and FEDER program (SINFOTON2-CM: P2018/NMT-4326).

Acknowledgment. The authors would like to thank Karen Delplace and Andy Cassez for supporting the realization of optical fibers and Rémi Habert and Stéphane Plus for the characterization of the obtained fibers. The IRCICA website is at https://ircica.univ-lille.fr

Disclosures. The authors declare no conflicts of interest.

Data availability. Data underlying the results presented in this paper are not publicly available at this time but may be obtained from the authors upon reasonable request.

REFERENCES

1. L. Alwis, T. Sun, and K. Grattan, "Optical fibre-based sensor technology for humidity and moisture measurement: Review of recent progress," Measurement **46**, 4052 (2013).
2. X. Bao and L. Chen, "Recent progress in distributed fiber optic sensors," Sensors **12**, 8601 (2012).
3. X. Lu, P. J. Thomas, and J. O. Hellevang, "A review of methods for fibre-optic distributed chemical sensing," Sensors **19**, 2876 (2019).
4. U. Uyor, A. Popoola, O. Popoola, and V. Aigbodion, "Polymeric cladding materials under high temperature from optical fibre perspective: a review," Polym. Bull. **77**(3), 2155 (2020).
5. D. Gloge, "Optical-fiber packaging and its influence on fiber straightness and loss," Bell Syst. Tech. J. **54**, 245 (1975).
6. P. Giaccari, H. Limberger, and P. Kronenberg, "Influence of humidity and temperature on polyimide-coated fiber Bragg gratings," in *Bragg Gratings, Photosensitivity, and Poling in Glass Waveguides* (Optical Society of America, 2001), paper BFB2.
7. C. Galíndez, F. Madruga, M. Lomer, A. Cobo, and J. López-Higuera, "Effect of humidity on optical fiber distributed sensor based on Brillouin scattering," Proc. SPIE **7004**, 70044W (2008).
8. P. J. Thomas and J. O. Hellevang, "A fully distributed fibre optic sensor for relative humidity measurements," Sens. Actuators B Chem. **247**, 284 (2017).
9. T. Neves, R. Magalhães, L. Scherino, S. Martin-Lopez, H. F. Martins, P. Petagna, and L. Thévenaz, "Humidity effect on acrylate-and polyimide-coated fibres for distributed sensing applications," in *Optical Fiber Sensors* (Optical Society of America, 2020), paper T3-73.
10. P. Stajanca, K. Hicke, and K. Krebber, "Distributed fiberoptic sensor for simultaneous humidity and temperature monitoring based on polyimide coated optical fibers," Sensors **19**, 5279 (2019).
11. T. Neves, L. Scherino, J. C. Da Silva, R. Bernard, M. Bouet, K. Hey Tow, P. Petagna, and L. Thévenaz, "Distributed fibre optic thermo-hygrometer for monitoring the concrete curing," in *Optical Fiber Sensors* (Optical Society of America, 2022).
12. T. F. Neves, L. Zhang, F. Yang, K. H. Tow, P. Petagna, and L. Thévenaz, "A kilometre-range distributed relative humidity sensor," Proc. SPIE **11199**, 1119922 (2019).
13. C. P. Chawla, T. E. Bishop, D. M. Szum, and K. P. Murray, "New test method for determining the water sensitivity of optical fiber coatings," Opt. Eng. **30**, 763 (1991).
14. J. Pastor-Graells, H. Martins, A. Garcia-Ruiz, S. Martin-Lopez, and M. Gonzalez-Herraez, "Single-shot distributed temperature and strain tracking using direct detection phase-sensitive OTDR with chirped pulses," Opt. Express **24**, 13121 (2016).
15. S. C. Shit and P. Shah, "A review on silicone rubber," Natl. Acad. Sci. Lett. **36**, 355–365 (2013).
16. H. C. Hulst and H. C. van de Hulst, *Light Scattering by Small Particles* (Courier Corporation, 1981).
17. A. Masoudi and T. P. Newson, "Contributed review: Distributed optical fibre dynamic strain sensing," Rev. Sci. Instrum. **87**, 011501 (2016).
18. L. Thévenaz, *Advanced Fiber Optics* (EPFL, 2011).
19. W. Zhi, R. Guobin, L. Shuqin, and J. Shuisheng, "Loss properties due to Rayleigh scattering in different types of fiber," Opt. Express **11**, 39 (2003).
20. L. Palmieri and L. Schenato, "Distributed optical fiber sensing based on Rayleigh scattering," Open Opt. J. **7**, 104–127 (2013).
21. M. Barnoski and S. Jensen, "Fiber waveguides: a novel technique for investigating attenuation characteristics," Appl. Opt. **15**, 2112 (1976).
22. W. Eickhoff and R. Ulrich, "Optical frequency domain reflectometry in single-mode fiber," Appl. Phys. Lett. **39**, 693 (1981).
23. H. F. Taylor and C. E. Lee, "Apparatus and method for fiber optic intrusion sensing," U.S. patent5,194,847 (March 16, 1993).
24. X. Lu, "Coherent Rayleigh time domain reflectometry: Novel applications for optical fibre sensing," Ph.D. thesis (Ecole Polytechnique Fédérale de Lausanne, 2016).
25. Y. Koyamada, M. Imahama, K. Kubota, and K. Hogari, "Fiber-optic distributed strain and temperature sensing with very high measurand resolution over long range using coherent OTDR," J. Lightwave Technol. **27**, 1142 (2009).
26. M. R. Fernández-Ruiz, L. Costa, and H. F. Martins, "Distributed acoustic sensing using chirped-pulse phase-sensitive OTDR technology," Sensors **19**, 4368 (2019).

27. H. Gabai and A. Eyal, "SNR characterization in distributed acoustic sensing," Proc. SPIE **9916**, 99162W (2016).
28. M. R. Fernández-Ruiz, H. F. Martins, J. Pastor-Graells, S. Martin-Lopez, and M. Gonzalez-Herraez, "Phase-sensitive OTDR probe pulse shapes robust against modulation-instability fading," Opt. Lett. **41**, 5756 (2016).
29. R. Magalhães, J. Pereira, A. Garcia-Ruiz, W. Margulis, S. Martin-Lopez, M. Gonzalez-Herraez, and H. F. Martins, "Distributed detection of quadratic Kerr effect in silica fibers using chirped-pulse ε otdr," Proc. SPIE **11199**, 1119929 (2019).
30. R. Magalhaes, T. F. P. D. Neves, L. Scherino, S. Martin-Lopez, and H. F. Martins, "Reaching long-term stability in CP-OTDR," J. Lightwave Technol. **40**, 3916–3922 (2022).
31. R. Magalhães, T. Neves, L. Costa, L. Scherino, P. Petagna, L. Thevenaz, S. Martin-Lopez, M. Gonzalez-Herraez, and H. F. Martins, "Reaching mk-scale stability in cp-φ otdr over daily measurements," in *Optical Fiber Sensors Conference 2020 Special Edition* (Optica Publishing Group, 2020), paper T3.63.
32. C. Ishiyama and Y. Higo, "Effects of humidity on Young's modulus in poly (methyl methacrylate)," J. Polym. Sci. B **40**, 460 (2002).
33. A. Sarkar, S. Izadpanah, T. Bishop, C. Coady, J. Martin, and G. Pasternack, "High performance uv-cured optical fiber primary coating," Fiber Integr. Opt. **6**, 125 (1987).
34. F. Tsai, T. Blanton, D. Harding, and S. Chen, "Temperature dependence of the properties of vapor-deposited polyimide," J. Appl. Phys. **93**, 3760 (2003).